Ab initio study of structural stability of small 3d late transition metal clusters: Interplay of magnetization and hybridization

Ab initio study of structural stability of small 3*d* late transition metal clusters: Interplay of magnetization and hybridization

Soumendu Datta,[1] Mukul Kabir,[2] and Tanusri Saha-Dasgupta[1]

[1]*Advanced Materials Research Unit and Department of Material Sciences, S.N. Bose National Centre for Basic Sciences, JD Block, Sector-III, Salt Lake City, Kolkata 700 098, India*

[2]*Department of Materials Science and Engineering, Massachusetts Institute of Technology, Cambridge, Massachusetts 02139, USA*

(Received 25 March 2011; revised manuscript received 17 May 2011; published 5 August 2011)

Using first-principles density-functional-theory–based calculations, we analyze the structural stability of small clusters of 3*d* late transition metals. We consider the relative stability of the two structures: layer-like structures with hexagonal closed packed stacking and more compact structures of icosahedral symmetry. We find that the Co clusters show an unusual stability in hexagonal symmetry compared to the small clusters of other members, which are found to stabilize in icosahedral-symmetry–based structure. Our study reveals that this is driven by the interplay between the magnetic-energy gain and the gain in covalency through the *s*-*d* hybridization effect. Although we have focused our study primarily on clusters with 19 atoms, we find this behavior to be general for clusters with between 15 and 20 atoms.

DOI: 10.1103/PhysRevB.84.075429 PACS number(s): 73.22.−f, 36.40.Cg, 71.15.Mb

I. INTRODUCTION

Atomic clusters of nanometer size have attracted special attention in present-day research due to their applications in the fields of optoelectronics,[1,2] catalysis,[3,4] data storage,[5] sensors,[6–9] etc. The first step in the theoretical study of the properties of clusters is the determination of the minimum-energy structures. The equilibrium minimum-energy structures of small clusters often prefer compact geometries[10] like icosahedral- or cub-octahedral-symmetry–based structures. It has also been found in several cases that the deformed three-dimensional sections of the face centered cubic (fcc) or hexagonal closed packed (hcp) lattice appear as degenerate energy states or closely lying isomers.[11] However, depending on the local symmetry, they exhibit profoundly different properties. For example, planner gold clusters exhibit outstanding catalytic activity compared to their bulk counterpart of fcc symmetry,[12] and bilayer Ru nanoclusters exhibit significant chemical activity toward H_2O splitting compared to Ru clusters of hcp symmetry.[13] Similarly, the dependence of magnetic behavior of the Pd clusters on cluster symmetry is found to be significant.[14] All of these results indicate that the determination of the local symmetry is an unavoidable part in a cluster calculation.

In this article, we present a first-principles–based analysis to understand the structural trend of transition-metal clusters. Transition-metal clusters demand special attention because of their fascinating magnetic properties,[15,16] the dependence of their equilibrium structure on magnetism,[17] as well as their potential biomedical applications.[18–20] We focus our attention only on the 3*d* late-transition-metal clusters. Among the 3*d* late-transition-metal elements, Mn has a half-filled *d* level, while the others have a more than half-filled *d* level. Considering the earlier studies on structure of the 3*d* late-transition-metal clusters, it is seen that the small Mn and Fe clusters generally prefer a compact icosahedral growth pattern, as has been shown by first-principles calculations for Mn clusters[21–25] and Fe clusters.[26–29] For relatively less-magnetic Ni clusters and nonmagnetic Cu clusters, first-principles calculations and also some experimental evidence indicate mainly the icosahedral growth pattern.[30–34,35–40] Some recent calculations[41–43] also highlight the nonicosahedral or the amorphous structural pattern for small clusters of coinage metals like Cu, Ag, and Au. On the other hand, the ferromagnetic small cobalt cluster is quite different from the other members of the 3*d* late-transition-metal series, particularly Mn and Fe clusters. The small Co_n clusters rather prefer relatively noncompact layer-like structures. In our recent work[44] using first-principles density functional theory, we showed a clear hexagonal growth pattern for small Co_n clusters ($15 \leqslant n \leqslant 20$). Hexagonal-symmetry–based structures in this size range consist of three planes with hcp stacking. Also recently, this layer-like structure of small Co_n clusters ($13 \leqslant n \leqslant 23$) was reported by Gong *et al.*[45,46] using density functional calculations. However, experimental work on small Co_n clusters ($n < 50$)[47–49] is unable to give any definitive conclusion, which also indicates nonicosahedral packing.

It is therefore curious why the small cobalt clusters prefer an hcp growth pattern with layer-like stacking, while the clusters of the other 3*d* late-transition-metal elements apparently prefer a more compact icosahedral growth pattern. In order to gain an understanding of this issue, we choose these two close-packed structures with hcp and icosahedral symmetries as starting guesses and allow them to relax under the assumption of collinear magnetic ordering. We have studied the relative stability between these two symmetry-based structures in terms of energetics and structural and electronic properties. We have carried out our study for the entire series of 3*d* late-transition-metal clusters (i.e., Mn_n, Fe_n, Co_n, Ni_n, and Cu_n). Our study reveals that the contrasting behavior of the stability of Co clusters compared to the other members arises due to the interesting interplay of the effects of magnetization and hybridization.

II. COMPUTATIONAL DETAILS

We employed density functional theory with the plane-wave pseudopotential method as implemented in the Vienna *ab initio* simulation package.[50] We used the projected augmented

wave pseudopotentials[51,52] and the Perdew-Bruke-Ernzerhof exchange-correlation functional[53] of the generalized gradient approximation (GGA). The pseudopotentials for the transition-metal elements studied in this work were generated considering the $3d$ and $4s$ electrons as the valence electrons. The energy cutoff was 335 eV for the cluster calculation of each transition metal. We did both spin-polarized and non-spin-polarized calculations at the Γ point of the Brillouin zone. Geometry optimizations have been performed using the conjugate gradient and the quasi-Newtonian methods until all the force components were less than the threshold value of 0.01 eV/Å. For the cluster calculation, a simple cubic supercell was used with periodic boundary conditions, where two neighboring clusters were kept separated by around 12 Å vacuum space, which essentially makes the interaction between cluster images negligible. To determine the magnetic moment of the minimum-energy structure in spin-polarized calculations, we explicitly considered all the possible spin multiplicities for each structure under the approximation of collinear atomic spin arrangements.

III. RESULTS AND DISCUSSIONS

To make our conclusion regarding structural and electronic properties of the clusters more general, we have chosen the cluster size of 19 atoms for each $3d$ late-transition-metal cluster considered in this study, instead of the cluster size of 13 atoms, which is the first geometric magic size for the icosahedral-symmetry–based structure of most transition-metal clusters. Figure 1 shows the cluster structures of 19 atoms with hcp and icosahedral symmetries. A 19-atom-cluster structure with hcp symmetry can be viewed as a stacking of three planes containing 6, 7, and 6 atoms, respectively, in each of these planes. On the other hand, a 19-atom-cluster structure with icosahedral symmetry can be thought of as two interpenetrating 13-atom icosahedrons. As seen from Fig. 1, a 19-atom-cluster structure of hcp symmetry appears more open in the sense that is has a smaller value of the average coordination of atoms, as well as a more layer-like structure compared with the 19-atom icosahedral structure. In the first step of our optimization procedure, we have started with ideal hexagonal and icosahedral structures for 19-atom clusters and have optimized them. In the second step, we have randomly displaced a few atoms in the optimized structure obtained in the first step and have re-optimized to get the "final optimized" structure. The second step has been carried out considering all possible collinear spin arrangements of the atomic spins in each X_{19} (X = Mn, Fe, Co, Ni, Cu) cluster within the spin-polarized calculation. The optimized clusters do not have perfect hexagonal or icosahedral symmetry but are heavily distorted.

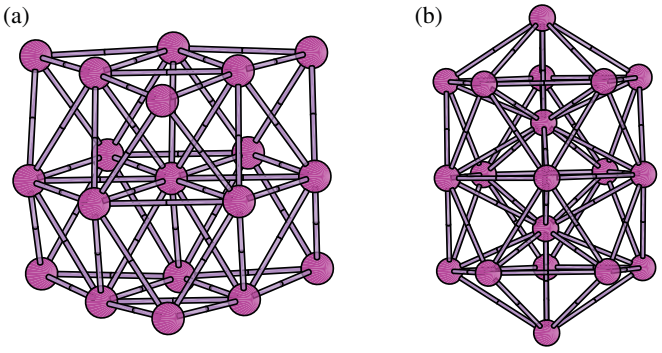

FIG. 1. (Color online) Cluster structures of 19 atoms with (a) hexagonal closed packed and (b) icosahedral symmetries. These two competing structural symmetries have been considered in this work to determine the minimum-energy structure for each X_{19} cluster; X = Mn, Fe, Co, Ni, and Cu.

First, to analyze the optimized structures, we define the average nearest-neighbor bond length as $\langle r \rangle = \frac{1}{n_b} \sum_{i>j} r_{ij}$, where r_{ij} is the bond distance between the jth and ith atoms and n_b is the number of such bonds. In the cluster calculation, we considered that the two atoms are bonded if their interatomic distance is within 2.75 Å, which is larger than any of the nearest-neighbor bulk bond lengths of these $3d$ late-transition-metal elements. Figure 2 shows the plot of the average nearest-neighbor bond-lengths of the optimized structures of X_{19} clusters for both symmetries. It is seen that the average nearest-neighbor bond lengths for the hcp structures are consistently smaller than those of the icosahedral counterpart, in agreement with the previous study[54] which indicates that the net attraction of nucleus on outer shell electrons is effectively greater for the hcp-symmetry–based structure. As the d shell gets filled one by one with electrons from Mn → Fe → Co → Ni → Cu, the ion-electron interaction gets stronger, which increases the binding. On the other hand, electron-electron repulsion also increases, which starts to downplay the gain in electron-ion attraction. On top of this effect, the increased atom-centered magnetic moments also play a significant role, especially for the members left of Co along Co_{19} to Fe_{19} to Mn_{19}.

In Fig. 3, we show the average coordination number plotted for the optimized structures of X_{19} clusters in both symmetries.

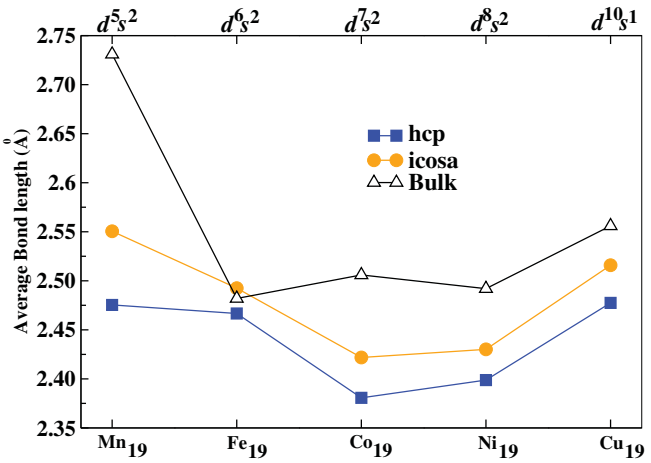

FIG. 2. (Color online) Plot of the average nearest-neighbor bond lengths ⟨r⟩ (see text) for the optimized hcp and icosahedral 19-atom clusters of Mn, Fe, Co, Ni, and Cu. Blue (dark) squares correspond to the datum points for the hcp structure and orange (light) circles for datum points of the icosahedral structure of each X_{19} cluster in the spin-polarized calculation. The corresponding bulk values have been shown with empty triangles. The atomic valance electronic configuration for each element has been marked at the top of the figure.

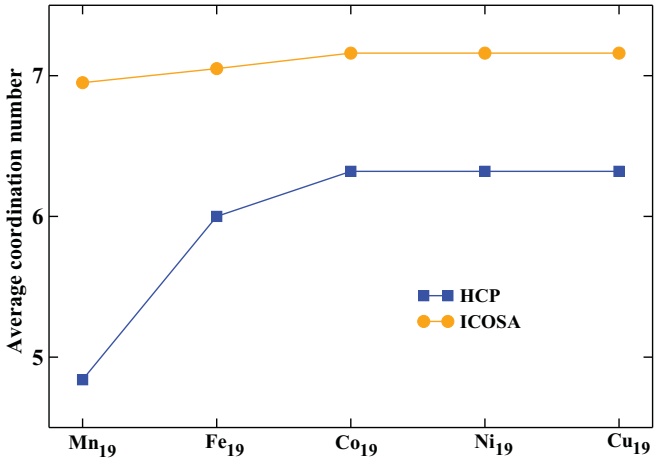

FIG. 3. (Color online) Plot of the average coordination number for the optimized hcp and icosahedral 19-atom clusters of Mn, Fe, Co, Ni, and Cu.

We find the average coordination for hcp-symmetry–based structures to be systematically less than that of icosahedral-symmetry–based structure, giving rise to a more open geometry, although the average bond length is smaller for hcp-based structures compared with icosahedral structures (cf. Fig. 2).

The binding energy for each X_{19} cluster is calculated as $E_B(X_{19}) = [19E(X) - E(X_{19})]$, where $E(X)$ and $E(X_{19})$ are the total energy of an isolated X atom and that of an X_{19} cluster, respectively. In such a definition, a positive sign in E_B corresponds to binding. Table I shows the total binding energy and the total magnetic moment of the optimized hcp and icosahedral structures of each X_{19} cluster. It is seen that the icosahedral-symmetry–based structure is more stable than the hcp-symmetry–based structure for Mn_{19} and Fe_{19} clusters. Conversely, the hcp-symmetry–based structure is energetically more favorable than the icosahedral structure for the Co_{19} cluster, while both structures are almost degenerate for the Ni_{19} and Cu_{19} clusters within the accuracy of our calculations. By analyzing the atomic spin orientations in the optimized structures of both symmetries of each X_{19} cluster, we found that the Mn-Mn interactions within the Mn_{19} cluster are mostly antiferromagnetic for both the optimal hcp and optimal icosahedral phases, as mentioned in earlier works.[21,24] On the other hand, each of the Fe_{19}, Co_{19}, and Ni_{19} clusters is ferromagnetic

TABLE I. Total binding energies and total magnetic moments of the minimum-energy structure of hcp and icosahedral symmetries for each X_{19} cluster, X = Mn, Fe, Co, Ni, and Cu in spin-polarized calculations.

	Binding Energy (eV)		Magnetic Moment (μ_B)	
Clusters	hcp	icosa	hcp	icosa
Mn_{19}	43.87	45.12	15	19
Fe_{19}	64.35	66.26	58	58
Co_{19}	72.01	70.80	39	37
Ni_{19}	65.13	65.13	18	14
Cu_{19}	47.04	46.95	0	0

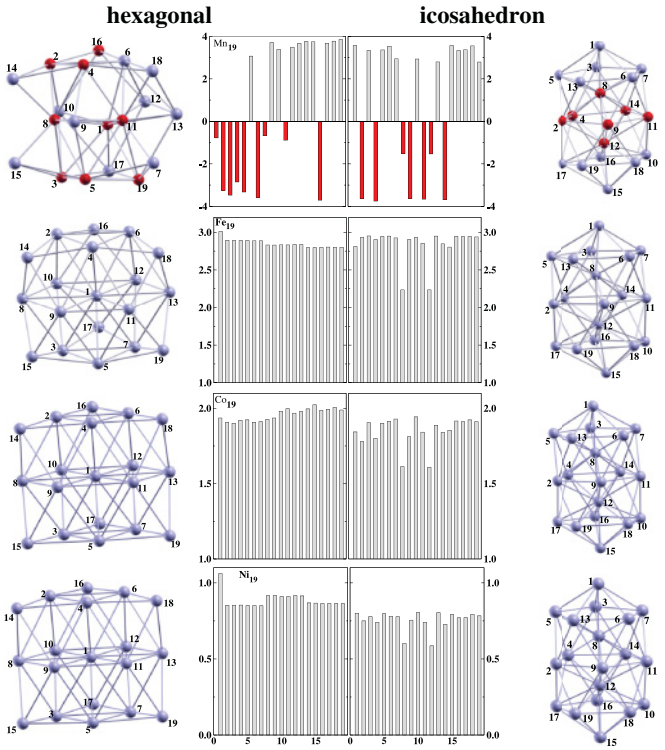

FIG. 4. (Color online) Structures and atomic magnetic moment (in μ_B) distribution in the optimized hcp and optimized icosahedral structures of Mn_{19}, Fe_{19}, Co_{19}, and Ni_{19} clusters in the spin-polarized calculation. For Mn_{19} clusters, the gray color represents up or positive and the red (dark gray) color represents down or negative magnetic moment. For each of Fe_{19}, Co_{19}, and Ni_{19} cluster, the atoms are ferromagnetically coupled, each with positive or up magnetic moments, and are, therefore, represented by same color (gray). The individual atomic magnetic moments of the constituent atoms in each optimized structure are represented by bar plots where the length of the bars corresponds to the magnitude of atomic moments. The numbering of the atoms in each structure is indicated in the plots of the structures shown in the side columns.

for either of the two structural symmetries, with decreasing total magnetic moment because the atom-centered magnetic moments decrease as one goes along $Fe_{19} \rightarrow Co_{19} \rightarrow Ni_{19}$. Figure 4 shows the distribution of atomic magnetic moments of each of the X_{19} clusters derived from both symmetries together with the corresponding optimized structures. Note that bulk Mn is also antiferromagnetic and bulk Fe, Co, and Ni are ferromagnetic (with a magnetic moment per atom of $2.2\mu_B$ for Fe,[55,56] $1.72\mu_B$ for Co,[56] and $0.616\mu_B$ for Ni[57]). The Cu_{19} cluster is found to be nonmagnetic with zero magnetic moment.

To have a visual representation, we plot the binding energy per atom for the optimal hcp and optimal icosahedral structures of each X_{19} cluster in Fig. 5. To understand the effect of magnetism on stability, we have also performed the non-spin-polarized calculation for each X_{19} cluster. The binding energies for the optimal hcp and icosahedral structures of X_{19} clusters in the non-spin-polarized calculation are also shown in Fig. 5 (right panel) with shaded bars. Interestingly, the non-spin-polarized calculation shows that the Mn_{19}, Fe_{19}, and Co_{19} clusters all stabilize in hcp-symmetry–based structures,

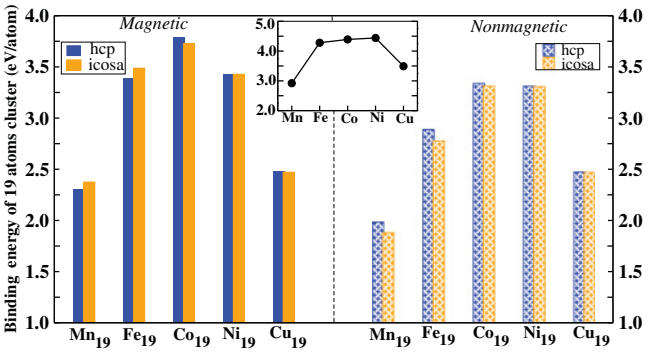

FIG. 5. (Color online) Plot of binding energy per atom of the minimum-energy hcp and icosahedral structures for each $X_{19}(X =$ Mn, Fe, Co, Ni, Cu) cluster in both the spin-polarized calculation (left) and the non-spin-polarized calculation (right). The blue (dark) vertical bars correspond to binding energies of the minimum-energy hcp structure and the vertical orange (light) bars correspond to the binding energies of the minimum-energy icosahedral structure. The inset shows the trend in the bulk binding energy per atom for Mn, Fe, Co, Ni, and Cu.

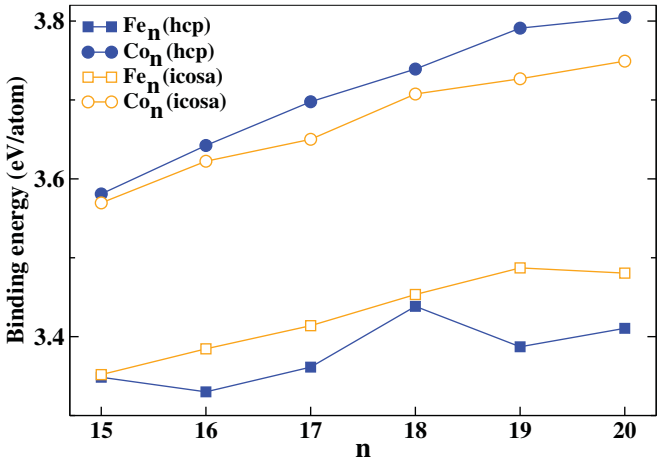

FIG. 6. (Color online) Plot of binding energies of minimum-energy hcp and icosahedral structures for each Fe_n and Co_n cluster ($15 \leqslant n \leqslant 20$) in the spin-polarized calculations. The squares correspond to the datum points for the Fe_n clusters (solid squares for hcp symmetry and empty squares for icosahedral symmetry) and the circles for the datum points of Co_n clusters (solid circles for optimal hcp structure and empty circles for optimal icosahedral symmetry).

while both the structures are again degenerate for Ni_{19} and Cu_{19} clusters. From Fig. 5, it is also clearly seen that the magnetic phase always has the higher binding energy for both structures of each X_{19} cluster, indicating that the magnetic phase is the stable phase for both structures. Only in case of the Cu_{19} cluster is the binding energy of each structure the same for both the spin-polarized as well as the non-spin-polarized calculation, indicating that the Cu_{19} cluster is nonmagnetic. From the binding energy plot, we therefore conclude that the magnetism switches the stable phase from hcp to icosahedron in the case of the Mn_{19} and Fe_{19} clusters, while the magnetism further enhances the stability of the hcp phase for the Co_{19} cluster. For the Ni_{19} and Cu_{19} clusters, the effect of magnetism is small and both the hcp- as well as the icosahedral-symmetry–based structures are almost degenerate for both the spin-polarized as well as the non-spin-polarized calculations.

For Mn clusters, the effect of noncollinearity has been discussed in literature.[58] Mn is prone to noncollinearity due to the presence of the competing nature of magnetic interactions, although the degree of noncollinearity is found to decrease for cluster sizes larger than 13 atoms.[58] For Fe and Co clusters, the degree of noncollinearity is reported to be smaller yet compared to Mn.[59] Noncollinearity is favored by the magnetic energy associated with larger magnetic moments, which competes with chemical bonding energy. One would therefore expect a reduction of noncollinearity in moving to larger cluster size as well as in moving from Mn to Fe and Co. However, in order to check the influence of the possible noncollinearity which may arise due to competing magnetic interactions as well as the orbital component of the magnetic moment [driven by spin-orbit (SO) coupling], we have repeated our calculations for Fe_{19} and Co_{19} clusters in terms of GGA + SO calculations. The results obtained indicate that Fe_{19} and Co_{19} clusters are essentially collinear, with the degree of noncollinearity being less than 1°, in agreement with previously reported results.[59] Although the orbital components of magnetism are found to be finite ($\approx$0.08 μ_B), importantly the calculations carried out considering noncollinearity lead to only small changes in the binding-energy differences of the icosahedral and hexagonal geometries by 1%–2%, keeping the main conclusion of our study unchanged. In the following, we focus primarily on Fe_{19} and Co_{19} clusters, for which the switching of the stable phase between hcp and icosahedral structures occurs.

It is important to note that the trend in binding-energy calculation is very robust, being independent of the type of pseudopotential or of the nature of the exchange-correlation functional used in this study. We also found that this trend is general for clusters having sizes $15 \leqslant n \leqslant 20$.[60] The structures for $n = 15$, 16, 17, 18, and 20 were obtained by removing or adding atoms from the optimal 19-atom-cluster structure and then letting them optimize for all possible collinear spin configurations of the constituent atoms. In Fig. 6, we have shown a plot of binding energies of the optimal hcp and the optimal icosahedral structures of the Fe_n and Co_n clusters considering clusters sizes in the range $15 \leqslant n \leqslant 20$. It clearly indicates that the icosahedral growth pattern is more favorable for small Fe_n clusters and that the hcp growth pattern is more favorable for the small Co_n clusters in the spin-polarized calculations, in agreement with the trend observed for 19-atom clusters and discussed above. In Table II, we have also shown our estimated magnetic moments of the optimized hcp and icosahedral structures of Fe_n and Co_n clusters in this size range. Notice that our estimated magnetic moments for the optimized structures are in fair agreement with the recent result of Stern-Gerlach experiments for Fe clusters[61] and Co clusters.[62]

In order to understand the optimal structures and the distortions in the structure that arise during the optimization procedure, we list in Table III the root-mean-square (rms) distortion of the bond lengths in the optimized geometries,

TABLE II. Calculated magnetic moments of optimized hcp and icosahedral structures of Fe_n and Co_n clusters ($15 \leqslant n \leqslant 20$) in spin-polarized calculations. For comparison, we also list the recent experimental values (Ref. 61 for Fe_n clusters and Ref. 62 for Co_n clusters) of magnetic moments in this size range.

	M (μ_B/atom)				M (μ_B/atom)		
	Theory				Theory		
Clusters	hcp	icosa	Expt.	Clusters	hcp	icosa	Expt.
Fe_{15}	3.07	3.20	2.72	Co_{15}	2.07	1.93	2.38
Fe_{16}	3.13	3.13	2.94	Co_{16}	2.13	1.88	2.53
Fe_{17}	3.18	3.06	2.86	Co_{17}	2.06	2.06	2.24
Fe_{18}	3.11	3.11	3.02	Co_{18}	2.00	2.00	2.07
Fe_{19}	3.05	3.05	2.92	Co_{19}	2.05	1.95	2.21
Fe_{20}	3.00	3.00	2.73	Co_{20}	2.00	1.90	2.04

which gives us a feel of the distortions that accompany optimization.

The pertinent question, therefore, is what drives this phenomenon? To see the effect of magnetism, we first calculated the magnetic energy which is defined as the energy difference between the magnetic (spin-polarized) and nonmagnetic (non-spin-polarized) calculations for each of the hcp and icosahedral structures of X_{19} clusters, which were estimated for their optimal structures in magnetic and nonmagnetic calculations. Figure 7(a) shows the plot of magnetic energies of the X_{19} clusters for hcp- and icosahedral-symmetry–based optimal structures. It is interesting to note that the magnetic energy of the icosahedral structure is much higher than that of the hcp-symmetry–based structure for the Fe_{19} clusters (and also for the Mn_{19} cluster, although we do not bring it into our discussion due to the assumption of collinearity in our calculation, as mentioned before). On the other hand, it is of similar magnitude for the hcp-symmetry–based structure for the Co_{19} cluster and its icosahedral counterpart, with hcp being somewhat higher. The magnetic-energy difference between hcp and icosahedral structures is negligibly small in case of the Ni_{19} and Cu_{19} clusters. The zoomed plot around the Fe_{19} and Co_{19} datum points in Fig. 7(b) shows the effect of magnetic energy more closely, which shows opposite trends in magnetic-energy gain between Fe_{19} and Co_{19} more clearly. We note that the difference of magnetic-energy gains between the

TABLE III. Calculated rms deviations of bond lengths of Co_n and Fe_n clusters for $n = 15$ to 20 for both hcp- and icosahedral-symmetry–based optimized structures.

Magnetic Co_n clusters			Magnetic Fe_n Clusters		
Cluster	rms Distortion		Cluster	rms Distortion	
size	hcp	icosa	size	hcp	icosa
Co_{15}	0.036	0.073	Fe_{15}	0.100	0.075
Co_{16}	0.058	0.077	Fe_{16}	0.125	0.083
Co_{17}	0.054	0.110	Fe_{17}	0.129	0.076
Co_{18}	0.046	0.118	Fe_{18}	0.113	0.089
Co_{19}	0.043	0.073	Fe_{19}	0.121	0.096
Co_{20}	0.072	0.087	Fe_{20}	0.123	0.095

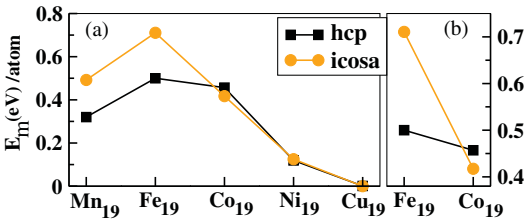

FIG. 7. (Color online) (a) Magnetic energy (E_m), calculated as the energy difference between the spin-polarized and non-spin-polarized calculations of the optimized hcp (solid squares) and icosahedral (light solid dots) structures plotted for each X_{19} cluster (X = Mn, Fe, Co, Ni, Cu). (b) Zoomed plot around the datum points for the Fe_{19} and Co_{19} clusters.

hcp and icosahedral structures in the case of the Co_{19} cluster is relatively small compared to that of the Fe_{19} cluster. As the d shell gets progressively filled up starting from the half-filled situation with the highest atom-centered magnetic moment for the Mn_n cluster, the magnetic-energy gain gets progressively weaker, so the role of magnetism is more important for Fe compared to Co.

In order to understand the gain in magnetic energy for the icosahedral structure of the Fe_{19} cluster and for the hcp structure of the Co_{19} cluster, we have studied the density of states (DOS) of the optimized hcp and icosahedral structures of the Fe_{19} and Co_{19} clusters for both the magnetic and nonmagnetic calculations, as shown in Fig. 8. We note that, compared to the nonmagnetic DOS, the gap in the majority-spin channel is significantly enhanced in case of the icosahedral structure of Fe_{19} and the hcp structure of Co_{19}, indicating their enhanced stability. On the other hand, for the optimal hcp structure of Fe_{19} and for the optimal icosahedral structure of Co_{19} clusters in case of the spin-polarized calculation, there is a finite number of states around the Fermi energy, which reduces the stability of the system compared to that of the corresponding icosahedral and hcp structures.

We next study another relevant quantity which has been used previously to examine the relative stability between the various classes of isomers for 3d late-transition-metal clusters; namely, the hybridization of the atomic 3d and 4s orbitals. The s-d hybridization index as quantified by Häkkinen *et al.*[63] and later used by Chang *et al.*[54] as well as Wang *et al.*[64] for transition-metal clusters is defined for a 19-atom cluster as

$$H_{sd} = \sum_{I=1}^{19} \sum_{i=1}^{\text{occ}} w_{i,s}^{(I)} w_{i,d}^{(I)},$$

where $w_{i,s}^{I}$ ($w_{i,d}^{I}$) is the projection of ith Khon-Sham orbital onto the s (d) spherical harmonic centered at atom I, integrated over a sphere of specified radius. The spin index is implicit in the summation. Our calculated s-d hybridization index for the optimized structures of both the symmetries for the Fe_{19} and Co_{19} and also for the Ni_{19} and Cu_{19} clusters have been plotted in Fig. 9. To see the effect of magnetism, we have studied the s-d hybridization of the optimized structure of each cluster for both the magnetic and nonmagnetic phases.

It is seen that the optimized hcp structures have consistently higher values of H_{sd} than those of the optimized icosahedral structures of 3d late-transition-metal clusters X_{19} for both

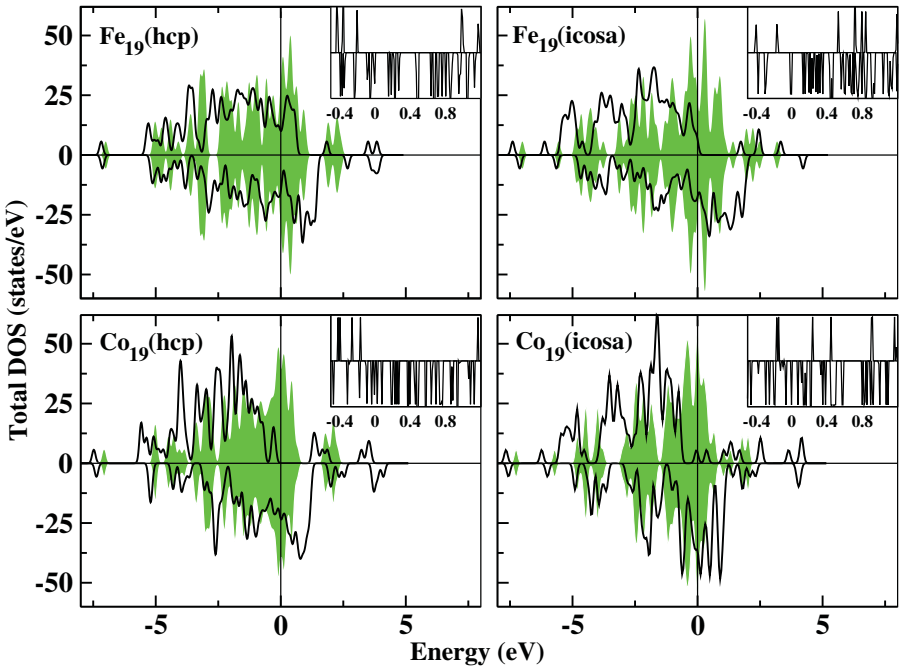

FIG. 8. (Color online) Plot of DOS of optimized hcp- and icosahedral-symmetry–based structures of Fe_{19} cluster (upper panels) and Co_{19} cluster (lower panels) in spin-polarized as well as non-spin-polarized calculations. The results for nonmagnetic calculations have been shown with shaded curves. The smearing width is fixed at 0.1 eV. The vertical line through zero is the Fermi energy for each system. The inset shows the DOS corresponding to the spin-polarized calculations, zoomed around the Fermi energy with a smearing of 0.001 eV.

spin-polarized and non-spin-polarized calculations. In order to see distinctly the effect of magnetization on *s-d* hybridization, we have plotted the difference of *s-d* hybridization indices between the optimized hcp and the optimized icosahedral structures for both the magnetic and nonmagnetic calculations in the right panel of Fig. 9. The positive (negative) value of this difference, $H_{sd}^{\rm diff}$, indicates that the hcp (icosahedron) structure has higher *s-d* hybridization. It is clearly seen that, although the difference is positive for all the late-transition-metal clusters, it shows some variation across the series. The *s-d* hybridization gain in favor of the hexagonal structure is the maximum for the magnetic Co_{19} cluster, showing a factor of about six-times enhancement compared to nonmagnetic Co_{19}. The Cu_{19} cluster being essentially nonmagnetic, the *s-d* hybridization gain between the two structural symmetries remains the same both in the magnetic and nonmagnetic calculation of Cu_{19}. The *s-d* hybridization gain remains similar for the magnetic Fe_{19} and nonmagnetic Fe_{19} ($H_{sd}^{\rm diff} \sim 0.3$) and that for magnetic Ni_{19} and nonmagnetic Ni_{19} ($H_{sd}^{\rm diff} \sim 0.4$). Therefore, we conclude that the gain in *s-d* hybridization stabilizes the hcp-symmetry–based structure over the icosahedral-symmetry–based structure for the Co_{19} cluster. This is also helped in a way by the small but positive magnetic-energy gain in favor of hcp phase of the Co_{19} cluster. So the *s-d* hybridization helped by magnetic-energy gain stabilizes the hcp-symmetry–based structure in the case of the Co_{19} cluster. On the other hand, for the Fe_{19} cluster, the large magnetic-energy gain in favor of the icosahedral symmetry decides the final stability, thereby counteracting the hybridization-energy gain in favor of hexagonal symmetry.

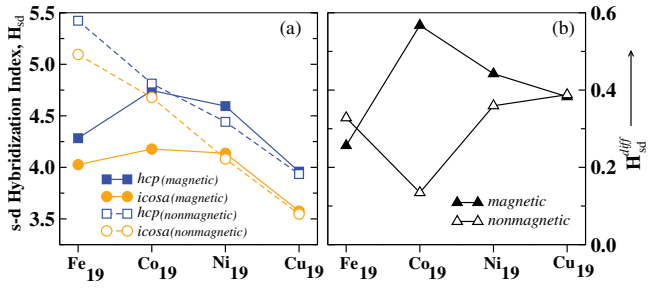

FIG. 9. (Color online) Plot of (a) *s-d* hybridization index for the optimized hcp and optimized icosahedral 19-atom clusters of Fe, Co, Ni, and Cu, both in the spin-polarized (magnetic) calculation and the non-spin-polarized (nonmagnetic) calculation (solid circles and squares represent the results for the spin-polarized calculation and empty circles and squares correspond to results for the non-spin-polarized calculations). (b) The difference in *s-d* hybridization ($H_{sd}^{\rm diff} = H_{sd}^{\rm hcp} - H_{sd}^{\rm icosa}$) between the optimized hcp and icosahedral structures of 19-atom clusters both in the spin-polarized and non-spin-polarized calculations.

IV. SUMMARY AND CONCLUSIONS

To summarize, we have investigated the relative stability of the 3*d* late-transition-metal clusters, especially of 19 atoms, between hcp and icosahedral symmetries. Among all the members, the Co_{19} cluster prefers an unusual stabilization in hexagonal symmetry, while the rest prefer icosahedral symmetry. Our study nicely demonstrates that this curious result is driven by the interplay of the gain in magnetic energy *vis à vis* the gain in hybridization energy. For the Co_{19} clusters, the hybridization-energy gain helped by magnetic-energy gain favors the stabilization of hexagonal symmetry while, for clusters like Fe_{19}, the large magnetic-energy gain in icosahedral symmetry topples the *s-d* hybridization gain in favor of hexagonal symmetry and stabilizes the icosahedral phase. We find that the trend obtained also holds good for clusters with between 15 and 20 atoms.

ACKNOWLEDGMENTS

T.S.D. and S.D. thank the Department of Science and Technology, India for support through Advanced Materials Research Unit.

[1] C. B. Murray, C. R. Kagan, and M. G. Bawendi, Science **270**, 1335 (1995).
[2] A. P. Alivisatos, Science **271**, 933 (1996).
[3] C. Coutanceau, S. Brimaud, C. Lamy, J. M. Leiger, L. Dubau, S. Rousseau, and F. Vigier, Electrochim. Acta **53**, 6865 (2008).
[4] A. Z. Moshfegh, J. Phys. D: Appl. Phys. **42**, 233001 (2009).
[5] G. Reiss and A. Hütten, Nat. Mater. **4**, 725 (2005).
[6] A. Kolmakov, X. Chen, and M. Moskovits, J. Nanosci. Nanotechnol. **8**, 111 (2008).
[7] W. Cha, M. R. Anderson, F. Zhang, and M. E. Meyerhoff, Biosens. Bioelectron. **24**, 2441 (2009).
[8] S. Wang, Q. Xu, X. Zhang, and G. Liu, Electrochem. Comm. **10**, 411 (2008).
[9] X. Luo, A. Morrin, P. J. Killard, and M. R. Smyth, Electroanalysis **18**, 319 (2006).
[10] J. A. Alonso, Chem. Rev. **100**, 637 (2000).
[11] J. Guevara, F. Parisi, A. M. Llois, and M. Weissmann, Phys. Rev. B **55**, 13283 (1997); A. N. Andriotis and M. Menon, *ibid.* **57**, 10069 (1998).
[12] M. D. Hughes, Yi-Jun Xu, Patrick Jenkins, Paul McMorn, Philip Landon, Dan I. Enache, Albert F. Carley, Gary A. Attard, Graham J. Hutchings, Frank King, E. Hugh Stitt, Peter Johnston, Ken Griffin, and Christopher J. Kiely, Nature (London) **437**, 1132 (2005).
[13] S. F. Li, Haisheng Li, Xinlian Xue, Yu Jia, Z. X. Guo, Zhenyu Zhang, and X. G. Gong, Phys. Rev. B **82**, 035443 (2010).
[14] F. Aguilera-Granja, J. M. Montejano-Carrizales, E. O. Berianga-Ramirez, and A. Vega, Phys. Lett. A **330**, 126 (2004).
[15] I. M. L. Billas, A. Chatelain, and W. A. de Heer, J. Magn. Magn. Mater. **168**, 64 (1997).
[16] M. B. Knickelbein, J. Chem. Phys. **125**, 044308 (2006).
[17] G. M. Pastor, R. Hirsch, and B. Mühlschlegel, Phys. Rev. Lett. **72**, 3879 (1994).
[18] O. V. Salata, J. Nanobiotech. **2**, 3 (2004).
[19] E. Duguet, S. Vasseur, S. Mornet, and J. Devoisselle, Nanomedicine **1**, 157 (2006).
[20] C. Riviere, S. Roux, O. Tillement, C. Billotey, and P. Perriat, Ann. Chim. (Paris) **31**, 351 (2006).
[21] M. Kabir, A. Mookerjee, and D. G. Kanhere, Phys. Rev. B **73**, 224439 (2006).
[22] Hannes Raebiger, Andres Ayuela, and J. von Boehm, Phys. Rev. B **72**, 014465 (2005).
[23] P. Bobadova-Parvanova, K. A. Jackson, S. Srinivas, and M. Horoi, J. Chem. Phys. **122**, 014310 (2005).
[24] T. M. Briere, M. H. F. Slutter, V. Kumar, and Y. Kawazoe, Bull. Mater. Sci. **26**, 115 (2003).
[25] Javier Guevara, Ana Maria Llois, F. Aguilera-Granja, and J. M. Montejano-Carrizales, Phys. Status Solidi **239**, 457 (2003).
[26] Masaki Sakurai, Koji Watanabe, Kenji Sumiyama, and Kenji Suzuki, J. Chem. Phys. **111**, 235 (1999).
[27] P. Bobadova-Parvanova, K. A. Jackson, S. Srinivas, and M. Horoi, Phys. Rev. B **66**, 195402 (2002).
[28] O. Diéguez, M. M. G. Alemany, C. Rey, Pablo Ordejón, and L. J. Gallego, Phys. Rev. B **63**, 205407 (2001).
[29] Brett I. Dunlap, Phys. Rev. A **41**, 5691 (1990); X. G. Gong and Q. Q. Zheng, J. Phys. Condens. Matter **7**, 2421 (1995).
[30] E. K. Parks, L. Zhu, J. Ho, and S. J. Riley, J. Chem. Phys. **100**, 7206 (1994).
[31] E. K. Parks, L. Zhu, J. Ho, and S. J. Riley, J. Chem. Phys. **102**, 7377 (1995).
[32] N. N. Lathiotakis, A. N. Andriotis, M. Menon, and J. Connolly, J. Chem. Phys. **104**, 992 (1996).
[33] N. N. Lathiotakis, A. N. Andriotis, M. Menon, and J. Connolly, Europhys. Lett. **29**, 135 (1995).
[34] S. K. Nayak, S. N. Khanna, B. K. Rao, and P. Jena, J. Phys. Chem. **101**, 1072 (1997).
[35] M. Kabir, A. Mookerjee, and A. K. Bhattacharya, Eur. Phys. J. D **31**, 477 (2004).
[36] J. Garcia-Rodeja, C. Rey, L. J. Gallego, and J. A. Alonso, Phys. Rev. B **49**, 8495 (1994).
[37] V. G. Grigoryan, D. Alamanova, and M. Springborg, Phys. Rev. B **73**, 115415 (2006).
[38] S. Darby, T. V. Mortimer-Jones, R. L. Johnson, and C. Roberts, J. Chem. Phys. **116**, 1536 (2002).
[39] B. J. Winter, E. K. Parks, and S. J. Riley, J. Chem. Phys. **94**, 8618 (1991).
[40] G. H. Guvelioglu, P. Ma, X. He, R. C. Forrey, and H. Cheng, Phys. Rev. Lett. **94**, 026103 (2005).
[41] J. Oviedo and R. E. Palmer, J. Chem. Phys. **117**, 9548 (2002).
[42] K. Michaelian, N. Rendon, and I. L. Garzón, Phys. Rev. B **60**, 2000 (1999).
[43] Q. L. Lu, Q. Q. Luo, L. L. Chen, and J. G. Wan, Eur. Phys. J. D **61**, 389 (2010).
[44] S. Datta, M. Kabir, S. Ganguly, B. Sanyal, T. Saha-Dasgupta, and A. Mookerjee, Phys. Rev. B **76**, 014429 (2007).
[45] S. F. Li, Haisheng Li, Xinlian Xue, Yu Jia, Z. X. Guo, Zhenyu Zhang, and X. G. Gong, Phys. Rev. B **82**, 035443 (2010).
[46] C. D. Dong and X. G. Gong, Phys. Rev. B **78**, 020409 (2008).
[47] M. Pellarin, B. Baguenard, J. L. Vialle, J. Lerme, M. Broyer, J. Miller, and A. Perez, Chem. Phys. Lett. **217**, 349 (1994).
[48] E. K. Parks, T. D. Klots, B. J. Winter, and S. J. Riley, J. Chem. Phys. **99**, 5831 (1993).
[49] E. K. Parks, B. J. Winter, T. D. Klots, and S. J. Riley, J. Chem. Phys. **96**, 8267 (1992).
[50] Vienna *ab initio* simulation package (VASP), Technische Universität Wien, 1999; G. Kresse and J. Hafner, Phys. Rev. B **47**, 558 (1993); G. Kresse and J. Furthmuller, *ibid.* **54**, 11169 (1996).
[51] P. E. Blöchl, Phys. Rev. B **50**, 17953 (1994).
[52] G. Kresse and D. Joubert, Phys. Rev. B **59**, 1758 (1999).
[53] J. P. Perdew, K. Burke, and M. Ernzerhof, Phys. Rev. Lett. **77**, 3865 (1996).
[54] C. M. Chang and M. Y. Chou, Phys. Rev. Lett. **93**, 133401 (2004).
[55] Isabelle M. L. Billas, J. A. Becker, A. Chatelain, and Walt A. de Heer, Phys. Rev. Lett. **71**, 4067 (1993).
[56] C. Kittel, *Introduction to Solid State Physics*, 5th ed. (Wiley, New York, 1986).
[57] Y. H. Yao, X. Gu, M. Ji, X. G. Gong, and Ding-sheng Wang, Phys. Lett. A **360**, 629 (2007).
[58] M. Kabir, D. G. Kanhere, and A. Mookerjee, Phys. Rev. B **75**, 214433 (2007).

[59]N. Fujima, J. Phys. Soc. Jpn. **71**, 1529 (2002); C. Zhi-Da, Z. Jing, and T. Zheng, Chin. Phys. Lett. **28**, 037501 (2011).

[60]Soumendu Datta, Ph.D. thesis, S. N. Bose National Centre for Basic Sciences, 2008.

[61]Mark B. Knickelbein, Chem. Phys. Lett. **353**, 221 (2002).

[62]X. Xu, S. Yin, R. Moro, and W. A. de Heer, Phys. Rev. Lett. **95**, 237209 (2005); M. B. Knickelbein, J. Chem. Phys. **125**, 044308 (2006).

[63]Hannu Häkkinen, Michael Moseler, and Uzi Landman, Phys. Rev. Lett. **89**, 033401 (2002); Hannu Häkkinen, Bokwon Yoon, and Uzi Landman, J. Phys. Chem. **107**, 6168 (2003).

[64]L.-L. Wang and D. D. Johnson, Phys. Rev. B **75**, 235405 (2007).